Supporting Information

Nitric oxide release by *N*-(2-chloroethyl)-*N*-nitrosoureas: a rarely discussed mechanistic path towards their anticancer activity

Amrita Sarkar,‡ Subhendu Karmakar,‡ Sudipta Bhattacharyya, Kallol Purkait and Arindam Mukherjee*[†]

[†]*Department of Chemical Sciences. Indian Institute of Science Education & Research Kolkata. Mohanpur. Nadia, Pin-741246, West Bengal, India. Fax: (+91)033-25873020. Tel: (+91)033-25873031. E-mail: a.mukherjee@iiserkol.ac.in*

Table of Contents

Table S1. Crystallographic data and structure refinement parameters for compound **1a**.

	1a
Empirical formula	$C_{12}H_{14}Cl_2N_6O_4$
F_w (g mol^{-1})	377.19
Temperature (K)	100(10)
Crystal system	triclinic
Space group	$P\bar{1}$
Crystal size/mm	0.798 × 0.587 × 0.475
a(Å)	8.9151(8)
b(Å)	9.8682(9)
c(Å)	10.9205(9)
α(°)	105.678(7)
β(°)	106.754(8)
γ(°)	108.541(8)
V(Å^3)	799.91(12)
Z	2
D_c (g cm^{-3})	1.566
μ (mm^{-1})	0.439
F(000)	388.0
Limiting indices	$-9 \leq h \leq 10$, $-11 \leq k \leq 8$, $-12 \leq l \leq 13$
Reflections collected	4599
Unique Reflections/R_{int}	2826/ 0.0268
Data/restraints/parameters	2826/0/217
Goodness-of-fit^a on F^2	1.052
$R_1{}^a$, $wR_2{}^b$ [I>2σ(I)]	R1 = 0.0408, wR2 = 0.0882
R_1,wR_2 (all data)	R1 = 0.0495, wR2 = 0.0940
$\Delta\rho_{max/min}$/ e Å^{-3}	0.34/-0.33

$^aR_1 = \Sigma\,(|F_o| - |F_c|)/|F_o|$. $^bwR_2 = [R\,[\Sigma\,(F_o^2 - F_c^2)^2]/R[\Sigma(F_o^2)^2]]^{1/2}$

Table S2. Selected bond distances (Å) and angles (°) of compound **1a**.

1a			
N(1)-C(1)	1.420(3)	C(10)- N(1)-C(1)	124.97(19)
N(1)-C(10)	1.341(3)	N(1)-C(10)-N(2)	114.3(2)
N(2)- C(10)	1.425(3)	C(6)-C(1)-N(1)	119.8(2)
N(2)- C(11)	1.461(3)	C(2)-C(1)-N(1)	120.8(2)
N(2)- N(3)	1.355(3)	C(10)-N(2)-C(11)	121.94(19)
N(4)-C(6)	1.430(3)	N(2)-C(11)-C(12)	112.66(19)
N(4)-C(7)	1.340(3)	N(3)-N(2)-C(10)	116.98(18)
N(5)-C(7)	1.424(3)	N(3)-N(2)-C(11)	121.09(18)
N(5)-C(8)	1.462(3)	N(4)-C(7)-N(5)	115.5(2)
N(5)-N(6)	1.352(3)	C(1)-C(6)-N(4)	123.0(2)
O(1)-C(10)	1.223(3)	C(5)-C(6)-N(4)	117.6(2)
O(3)-C(7)	1.224(3)	C(7)-N(4)-C(6)	124.0(2)
O(2)-N(3)	1.223(2)	N(5)-C(8)-C(9)	111.9(2)
O(4)-N(6)	1.224(3)	C(7)-N(5)-C(8)	121.24(19)
Cl(1)-C(12)	1.794(2)	N(6)-N(5)-C(7)	116.02(18)
Cl(2)-C(9)	1.788(3)	N(6)-N(5)-C(8)	121.78(19)
		O(1)-C(10)-N(1)	126.2(2)
		O(1)-C(10)-N(2)	119.4(2)
		O(2)-N(3)-N(2)	114.40(19)
		O(3)-C(7)-N(5)	118.7(2)
		O(3)-C(7)-N(4)	125.9(2)
		O(4)-N(6)-N(5)	114.18(19)
		C(11)-C(12)-Cl(1)	112.30(16)
		C(8)-C(9)-Cl(2)	110.87(18)

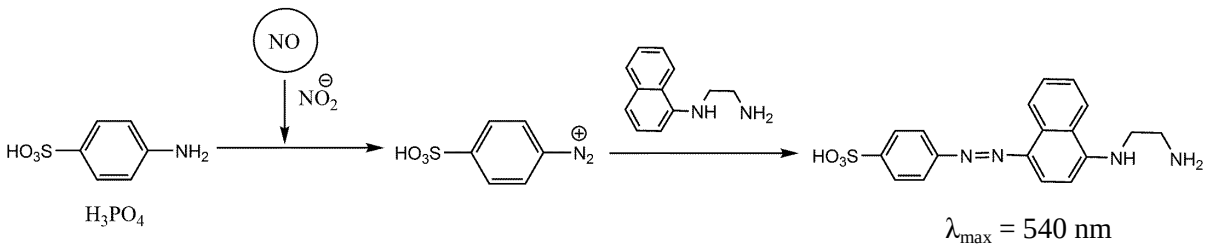

Scheme S1. Detection of nitrite (oxidized product of nitric oxide) in presence of Griess reagent system.

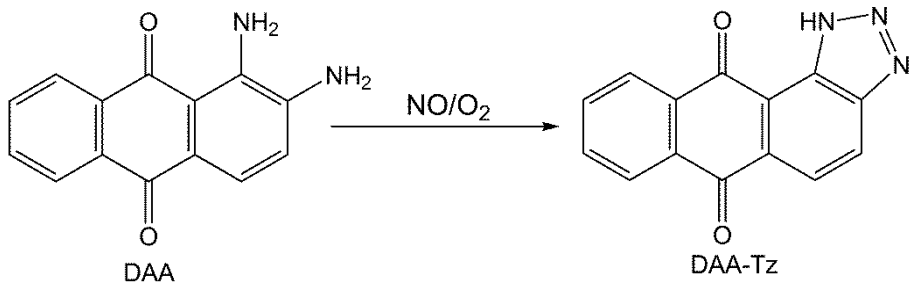

Scheme S2. Reaction between 1,2-diaminoanthraquinone (DAA) and nitric oxide (NO) in presence of O_2 to form triazole derivative of 1,2-diaminoanthraquinone (DAA-Tz)

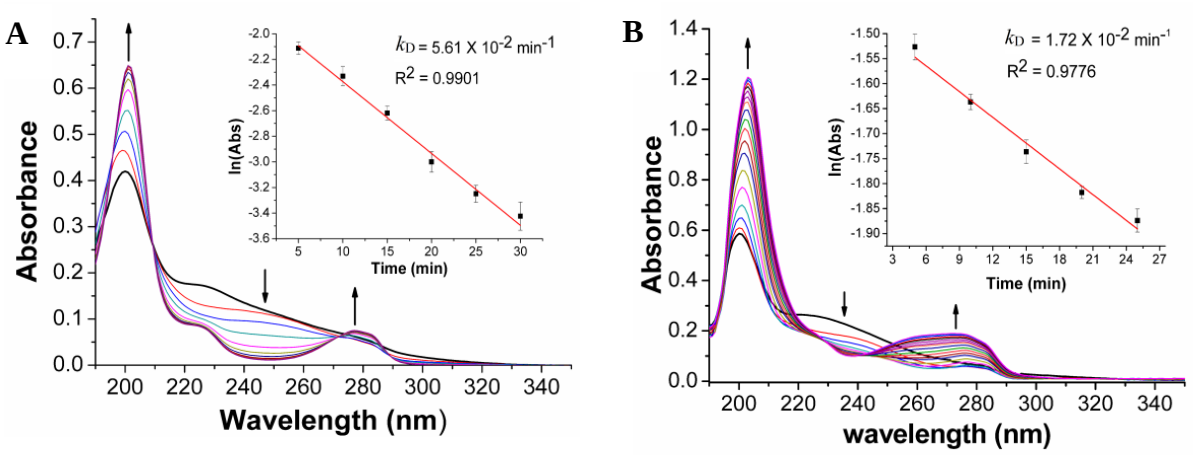

Fig. S1 UV-vis spectra for aqueous decomposition of **1a** in phosphate buffer (10 mM) at pH = 7.4 (A) and pH = 6.0 (B). Decrease in absorbance with time was recorded at λ = 236 nm. Inset: Linear fitting of ln(Abs) *vs*. time, from the slope rate of aqueous decomposition k_D and half life ($t_{1/2}$) were calculated. (T = 298K)

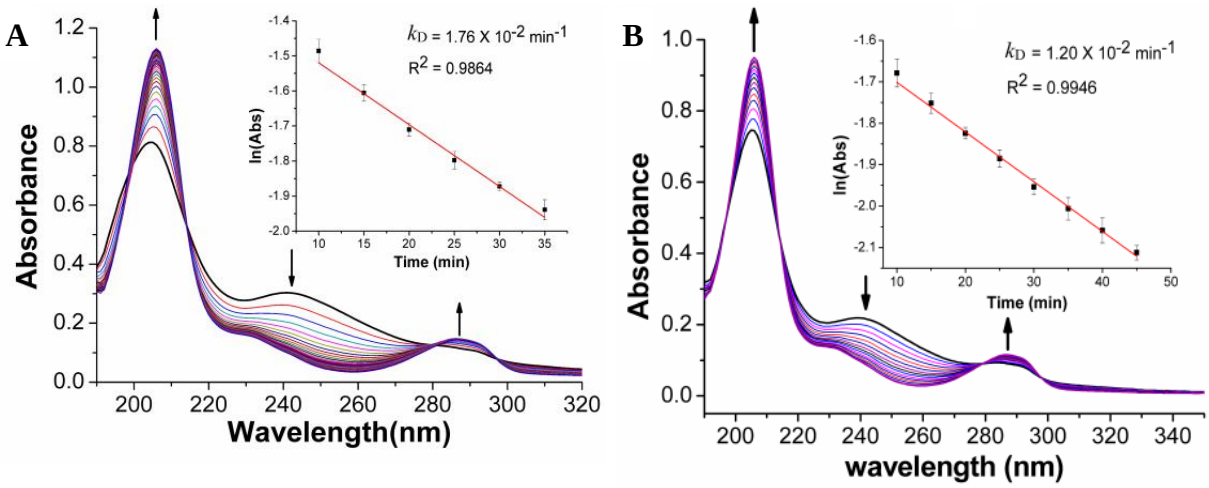

Fig. S2 UV-vis spectra of aqueous decomposition of **2a** in phosphate buffer (10 mM) at pH = 7.4 (A) and pH = 6.0 (B). Decrease in absorbance with time was recorded at λ = 242 nm. Inset: Linear fitting of ln(Abs) *vs*. time, the rate of aqueous decomposition k_D and half life ($t_{1/2}$) were calculated from the slope. (T = 298K)

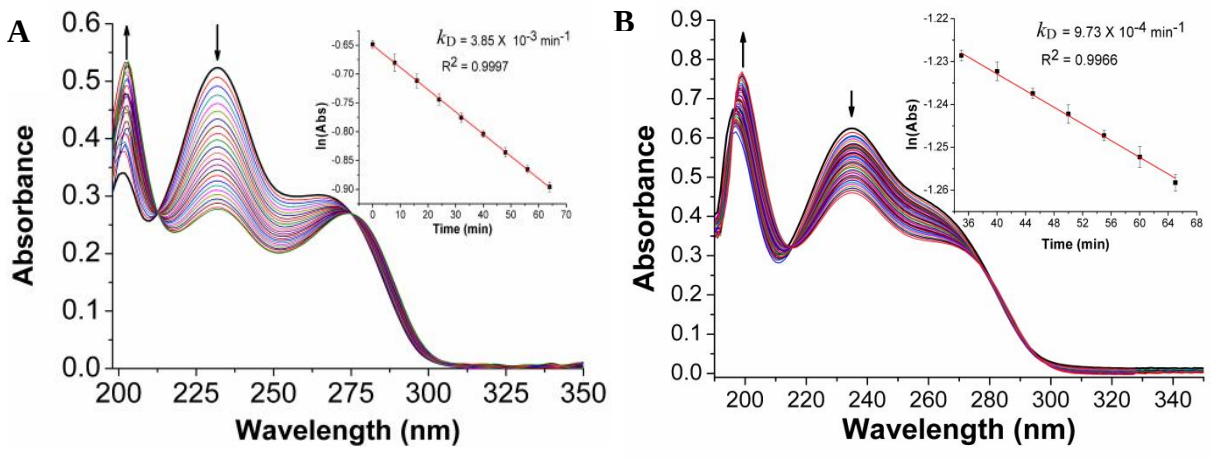

Fig. S3 UV-vis spectra for aqueous decomposition of nimustine hydrochloride in phosphate buffer (10 mM) at pH = 7.4 (A) and pH = 6.0 (B). Decrease in absorbance with time was recorded at λ = 232 nm. Inset: Linear fitting of ln(Abs) *vs*. time from which the rate of aqueous decomposition k_D and half life ($t_{1/2}$) were calculated. (T = 298K)

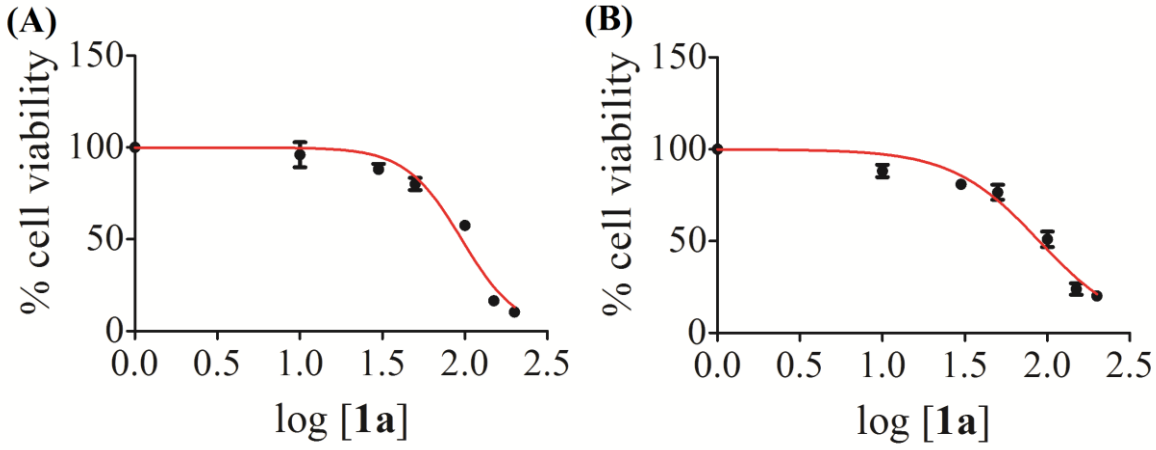

Fig. S4 Results of MTT assay of one independent experiment after treatment of MCF-7 tumor cell line with varying concentrations of **1a** for 48 h in normoxia (A) and hypoxia (B). The IC_{50} obtained from the curves are calculated using GraphPad Prism 5.0®. Data are mean ± SD of three independent experiments.

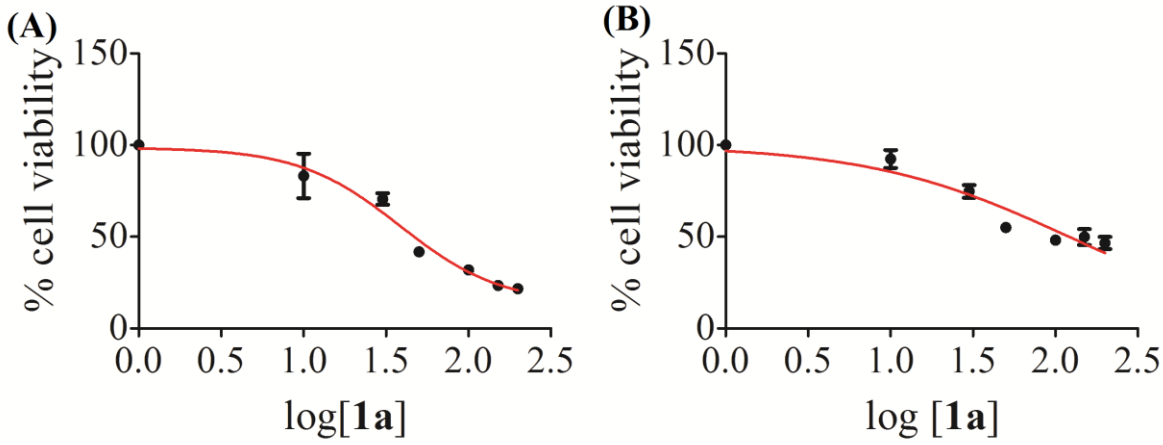

Fig. S5 Results of MTT assay of one independent experiment after treatment of A549 tumor cell line with varying concentrations of **1a** for 48 h in normoxia (A) and hypoxia (B). The IC_{50} obtained from the curves are calculated using GraphPad Prism 5.0®. Data are mean ± SD of three independent experiments.

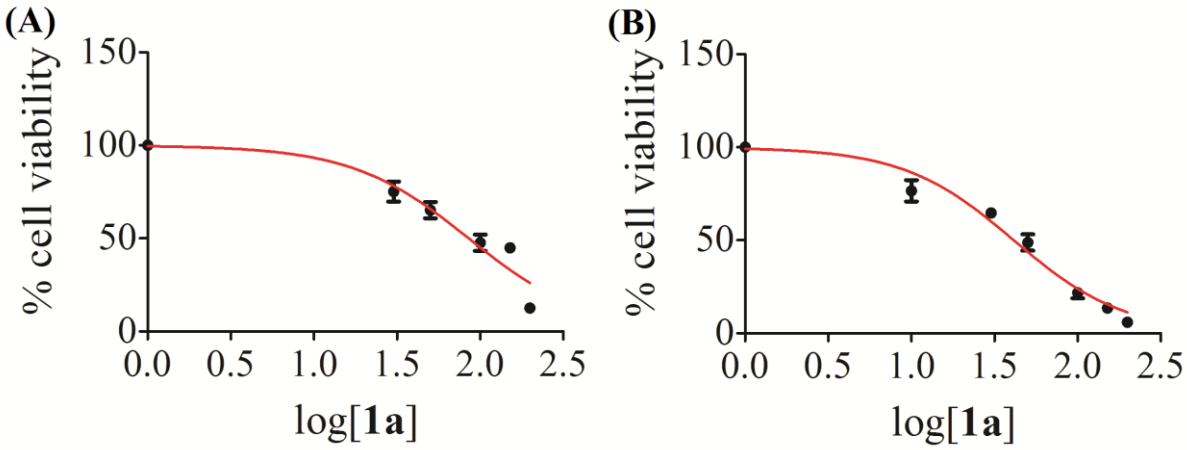

Fig. S6 Results of MTT assay with varying concentrations of **1a** in normoxia (A) HEK293T and (B) NIH3T3 cell lines. The IC_{50} obtained from the curves are calculated using GraphPad Prism 5.0®. Data are mean ± SD of three independent experiments.

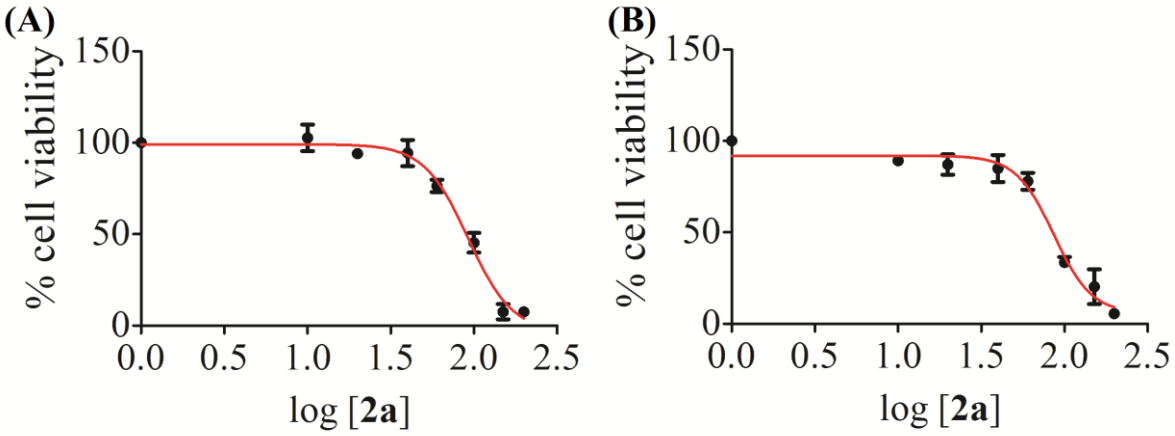

Fig. S7 Results of MTT assay of one independent experiment after treatment of MCF-7 tumor cell line with varying concentrations of **2a** in normoxia (A) and hypoxia (B). The IC_{50} obtained from the curves are calculated using GraphPad Prism 5.0®. Data are mean ± SD of three independent experiments.

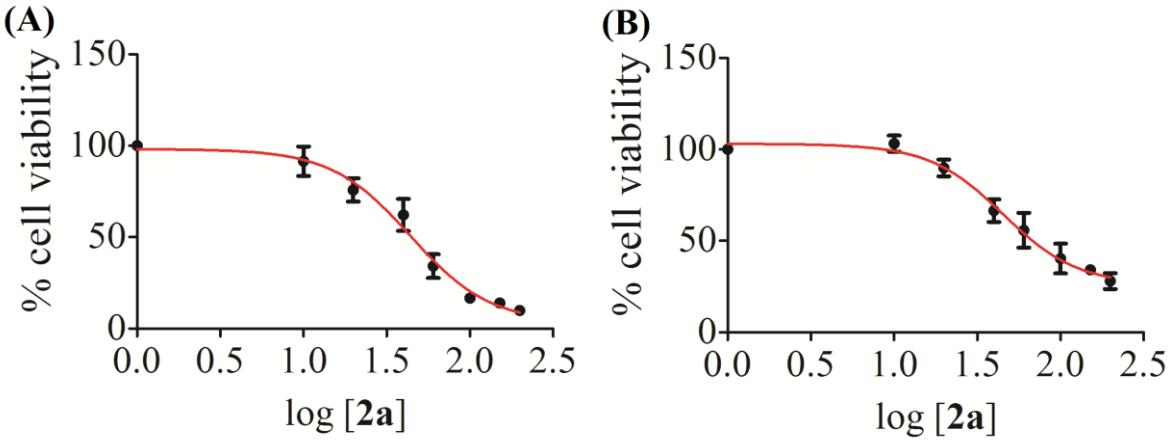

Fig. S8 Results of MTT assay of one independent experiment after treatment of A549 tumor cell line with varying concentrations of **2a** in normoxia (A) and hypoxia (B). The IC_{50} obtained from the curves are calculated using GraphPad Prism 5.0®. Data are mean ± SD of three independent experiments.

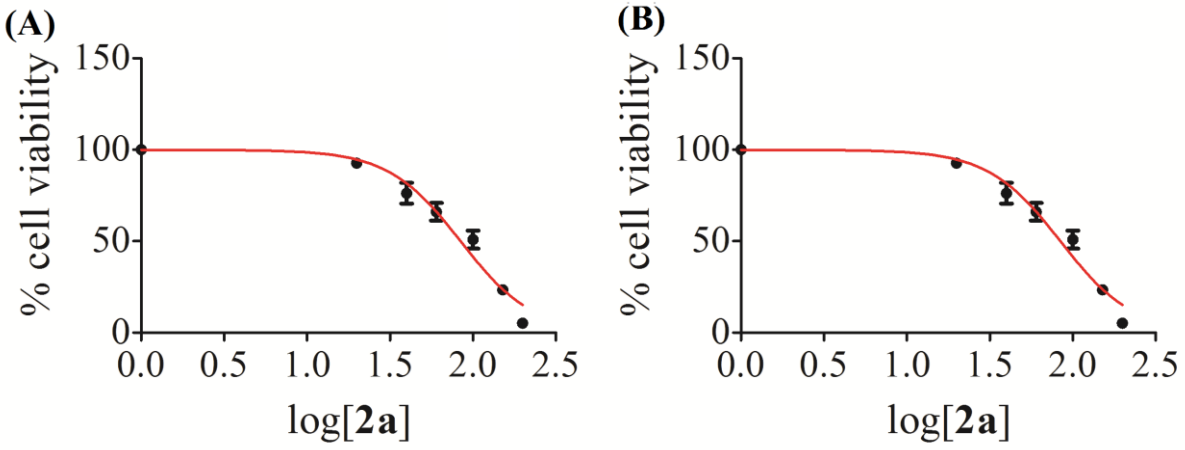

Fig. S9 Results of MTT assay of one independent experiment with varying concentrations of **2a** in normoxia (A) HEK293T and (B) NIH3T3 cell lines. The IC_{50} obtained from the curves are calculated using GraphPad Prism 5.0®. Data are mean ± SD of three independent experiments.

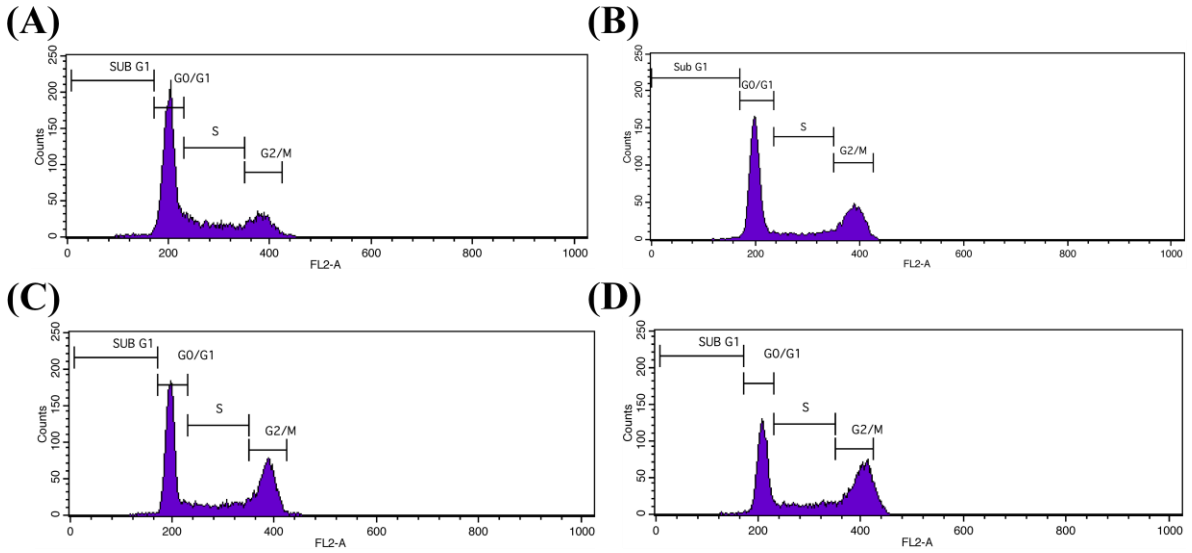

Fig. S10 Cell cycle analysis of A549 cells treated with (A) DMSO control, (B) 15 µM, (C) 25 µM, (D) 30 µM of **2a.**

Table S3. Cell cycle analysis of A549 cells with compounds **2a**. [a,b]

	Sub G1	**G0/G1**	**S**	**G2/M**
DMSO Control	1.1	62.8	20.4	15.7
2a (15 μM)	0.9	57.4	14.2	27.5
2a (25 μM)	0.4	54.9	12.1	32.6
2a (30 μM)	0.3	49.7	12.9	37.1

[a]Cells were treated for 24 h with **2a**. Cells were treated with propidium iodide and analyzed by FACS. Cell populations were analyzed and expressed as the percentage of cells in each phase. [b]The data presented is an average of two independent experiments.

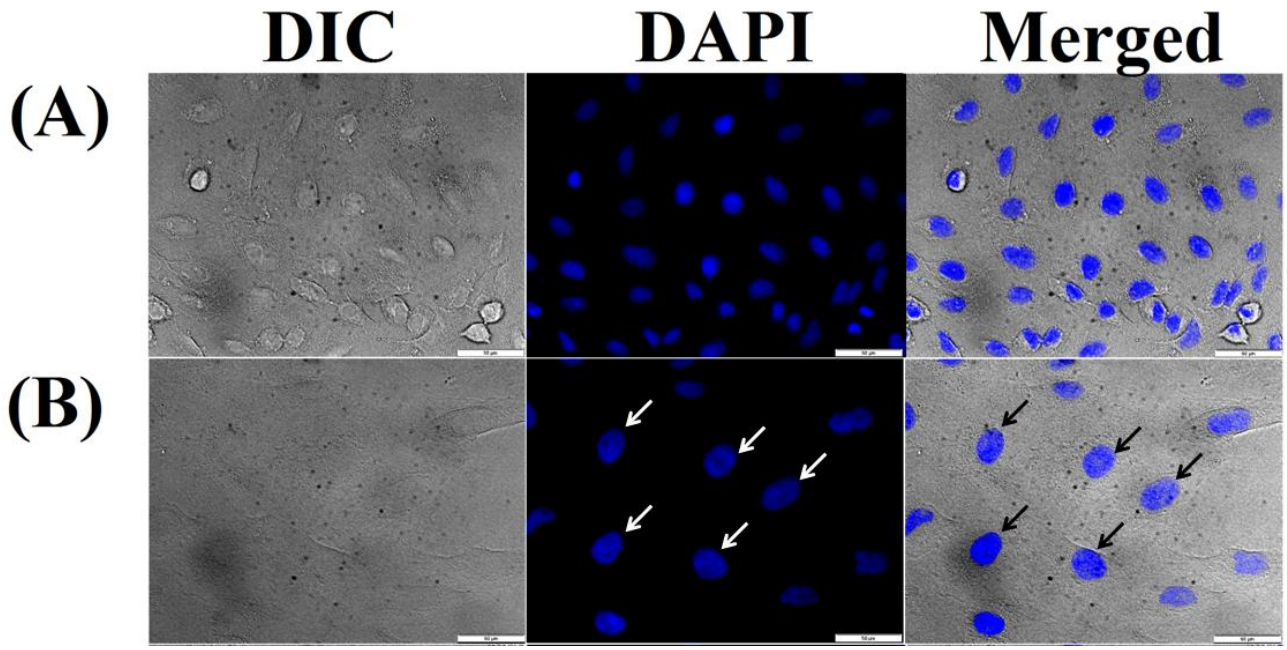

Fig. S11 Fluorescence microscopic images of A549 cells treated with **2a** for 24 h. DAPI was used as the DNA staining dye. Arrows show the nuclear morphological changes in cells upon treatment with **2a**. (A) DMSO treated (< 0.2%); (B) **2a** (15 μM).

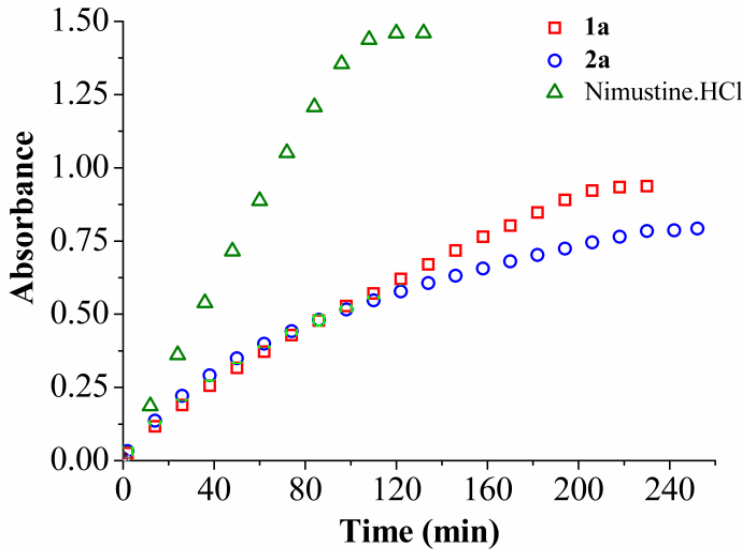

Fig. S12 Change in absorbance at λ_{max} = 540 nm with time for solution phase Griess reagent test for **1a**, **2a** and nimustine where the data points represents 12 min time interval.

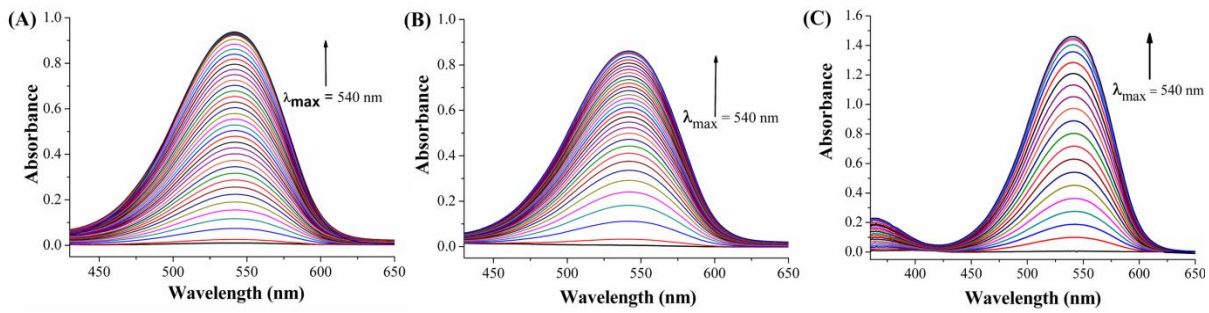

Fig. S13 Solution phase NO release study (λ_{max} = 540 nm) by (A) **1a**, (B) **2a** and (C) nimustine hydrochloride using Griess Reagent test.

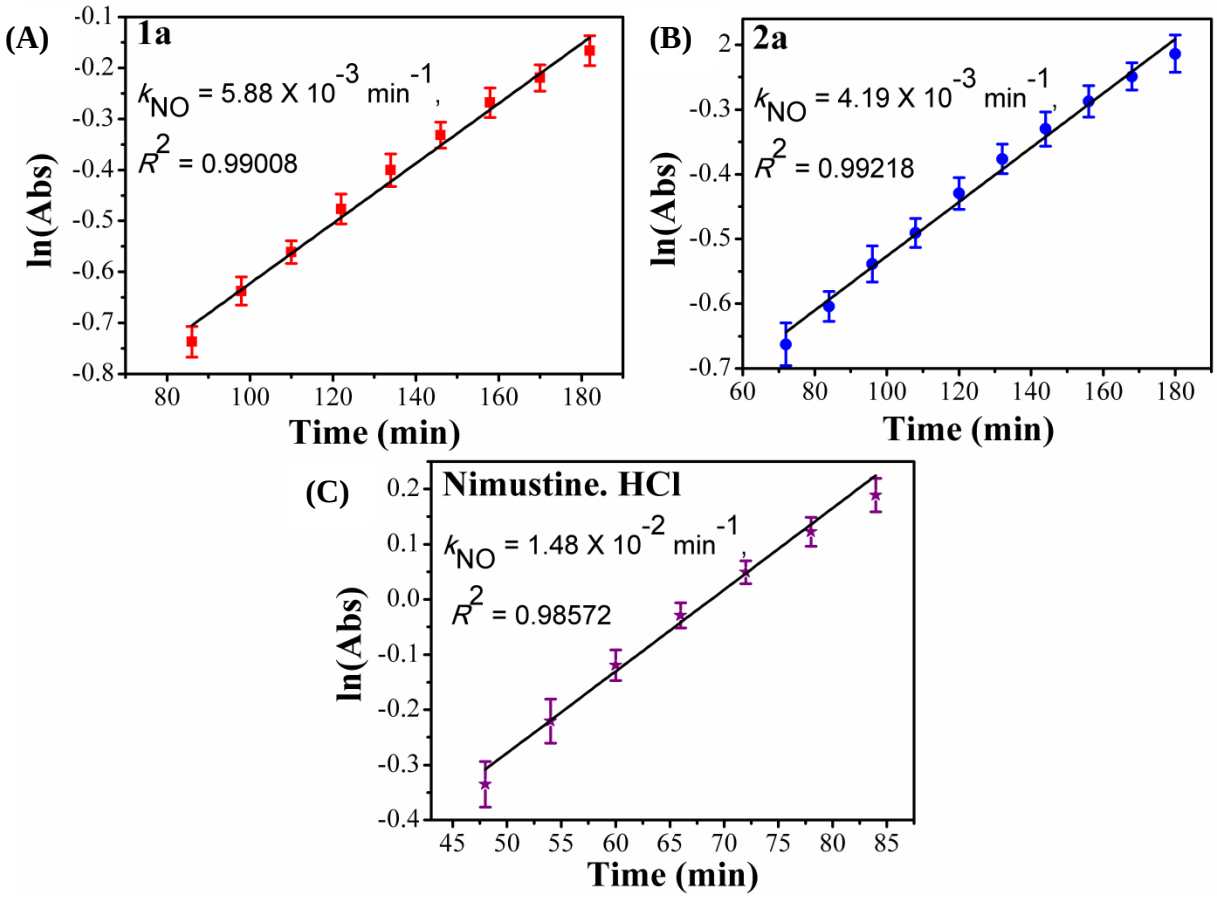

Fig. S14 The logarithmic plots of the absorbance λmax = 540 nm vs. time for calculating rate constant of NO release for compounds **1a**, **2a** and nimustine. (A) for **1a** (R2 = 0.99008), (B) for **2a** (R2 = 0.99218), (C) for nimustine.HCl (R2 = 0.99048) has been shown and the calculated rate constants are tabulated in Table 3.

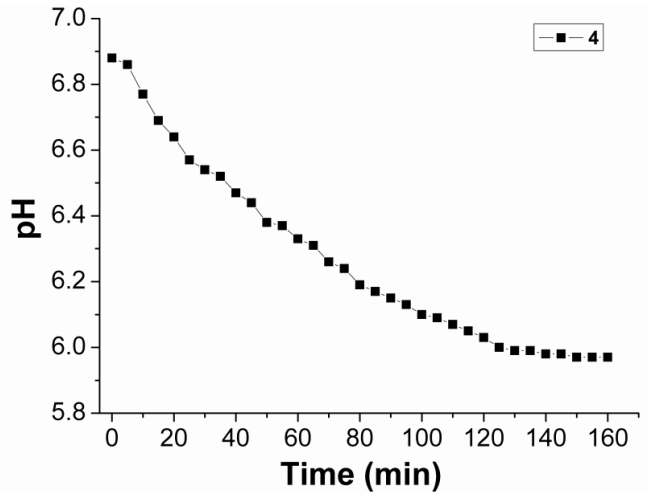

Fig. S15 Change in pH with time (0 – 160 min) of **1a** solution (10^{-2} M, 20% DMSO in H_2O).

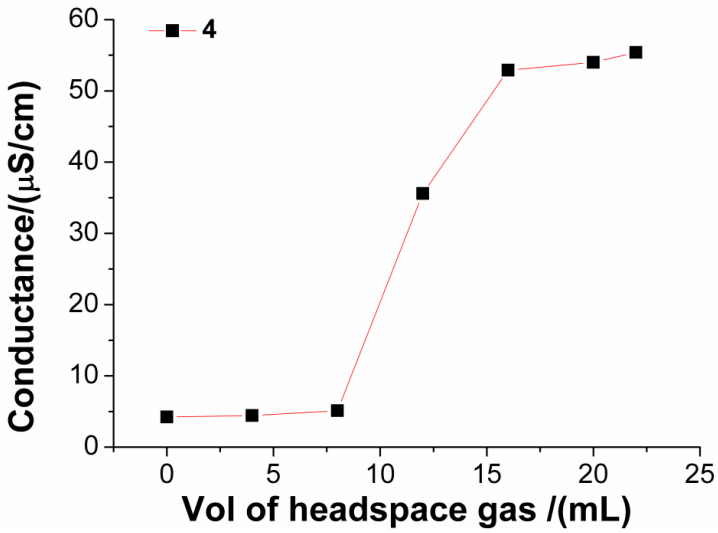

Fig. S16 Change in conductance of deionised water with increasing amount of headspace gas (purged) accumulated over the solution of **1a** (10 mM, 20% DMSO in H_2O)**.**

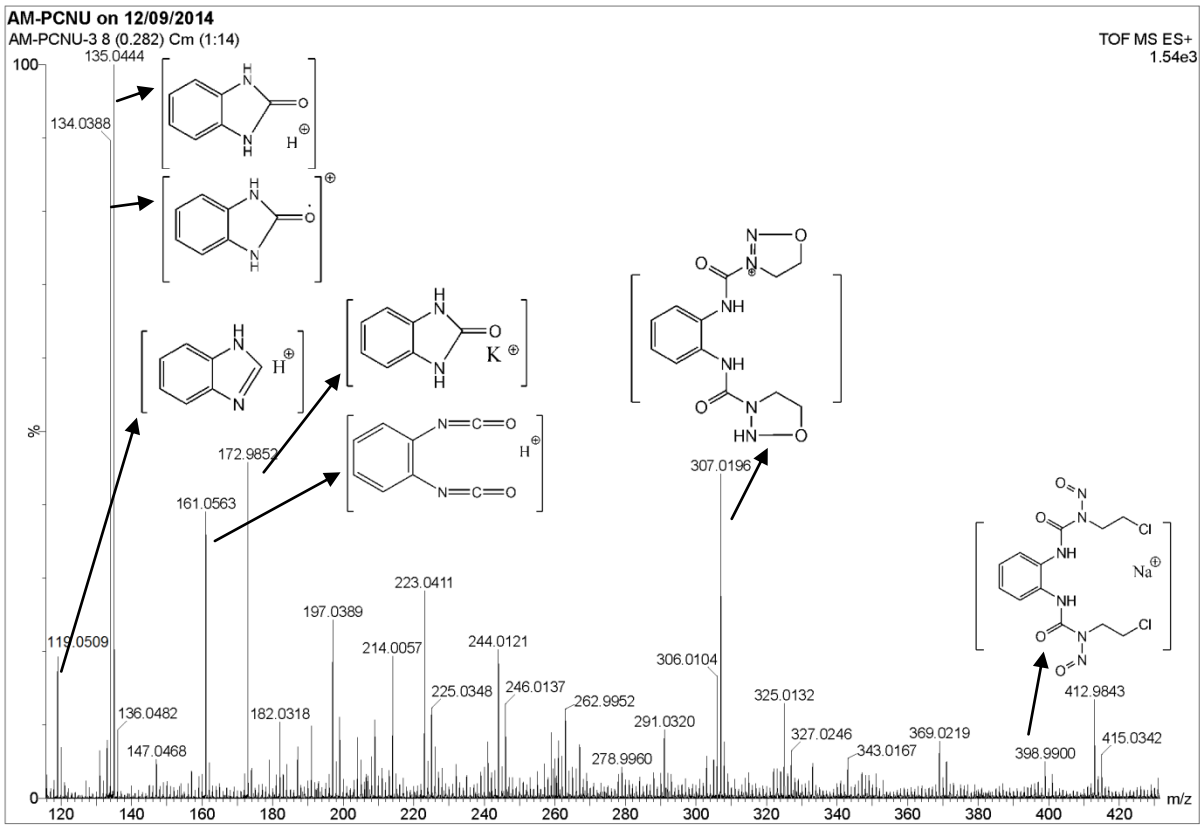

Fig. S17A ESI-MS (+ve ion mode) of **1a** in MeCN-H_2O mixture (2:1) where fragmentations are shown with arrows.

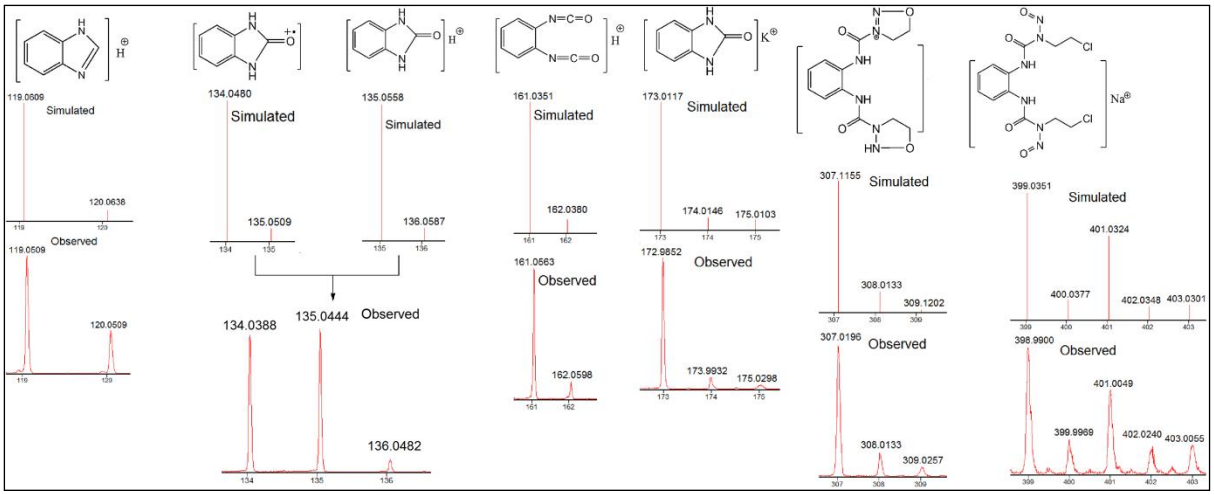

Fig. S17B Description of speciation of **1a** obtained in ESI-MS (+ ve mode) along with the isotopic distribution. A comparison of experimental and calculated values are provided.

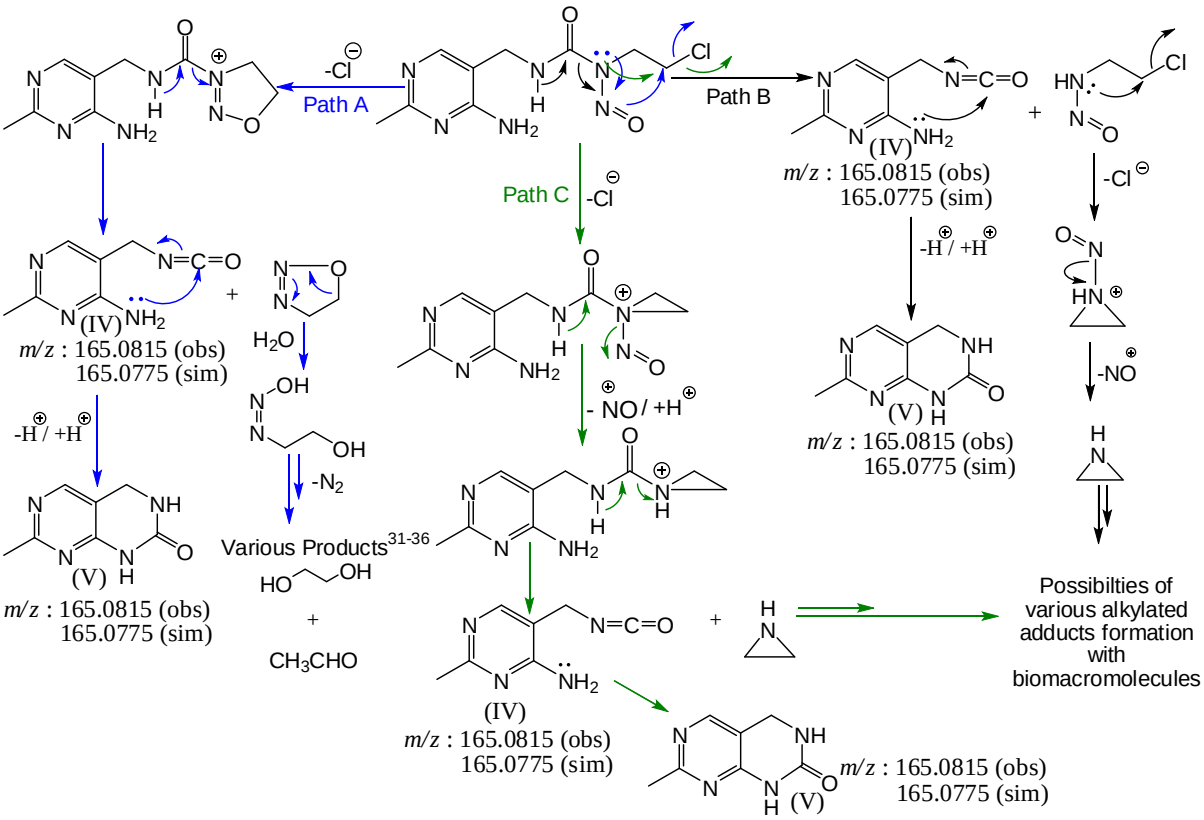

Scheme S3. Schematic representation of proposed mechanism of dissociation pathways for nimustine hydrochloride

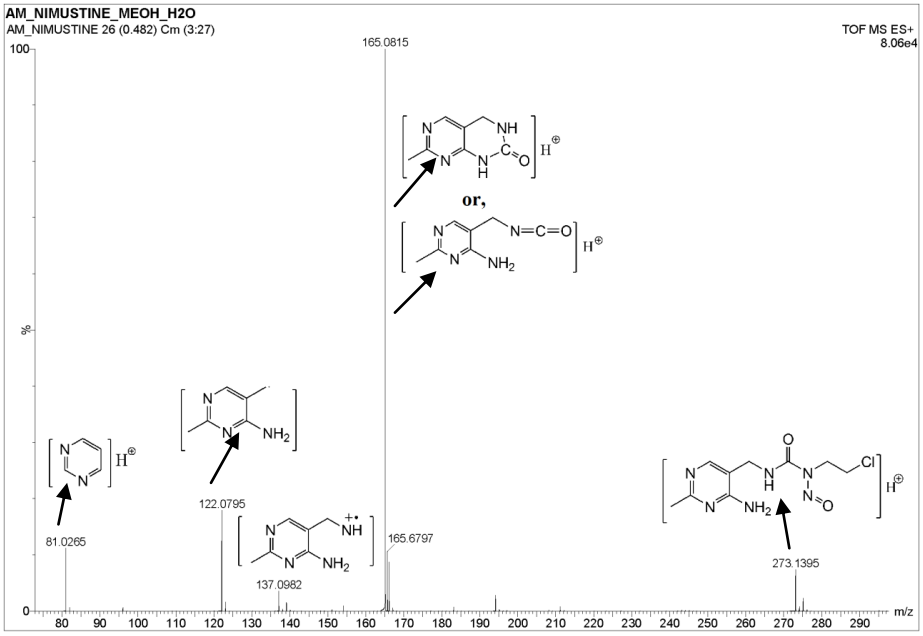

Fig. S18A ESI-MS (+ve ion mode) of nimustine hydrochloride in MeCN-H_2O mixture (2:1) where fragmentations are shown with arrows.

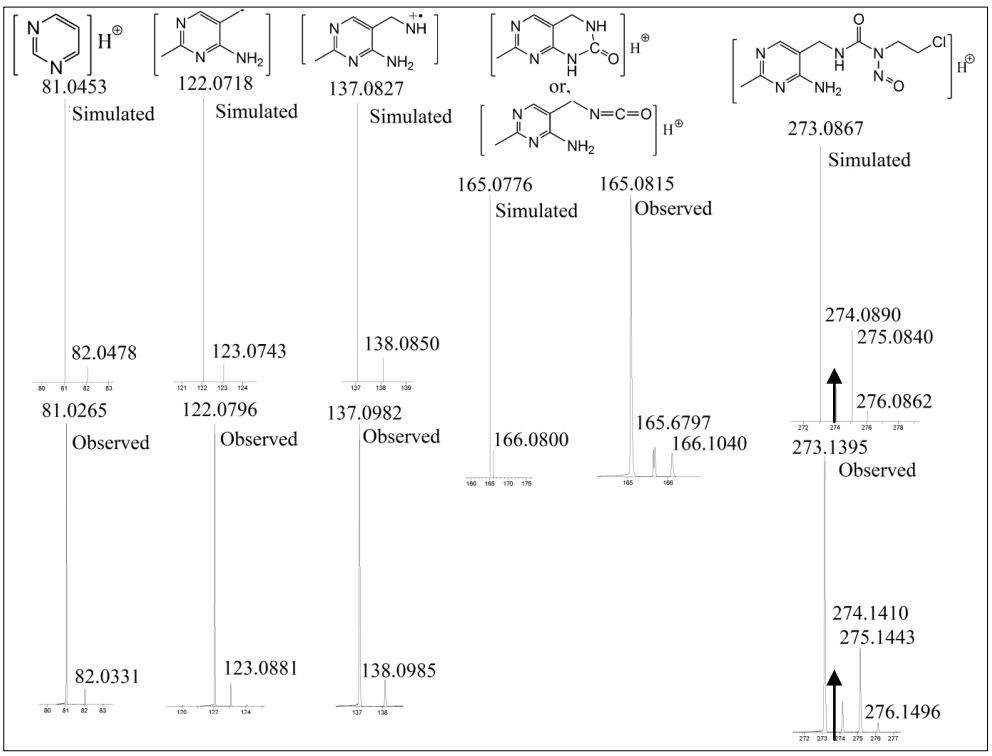

Fig. S18B Description of speciation of nimustine hydrochloride obtained in ESI-MS (+ ve mode) along with the isotopic distribution. A comparison of experimental and calculated values are provided.

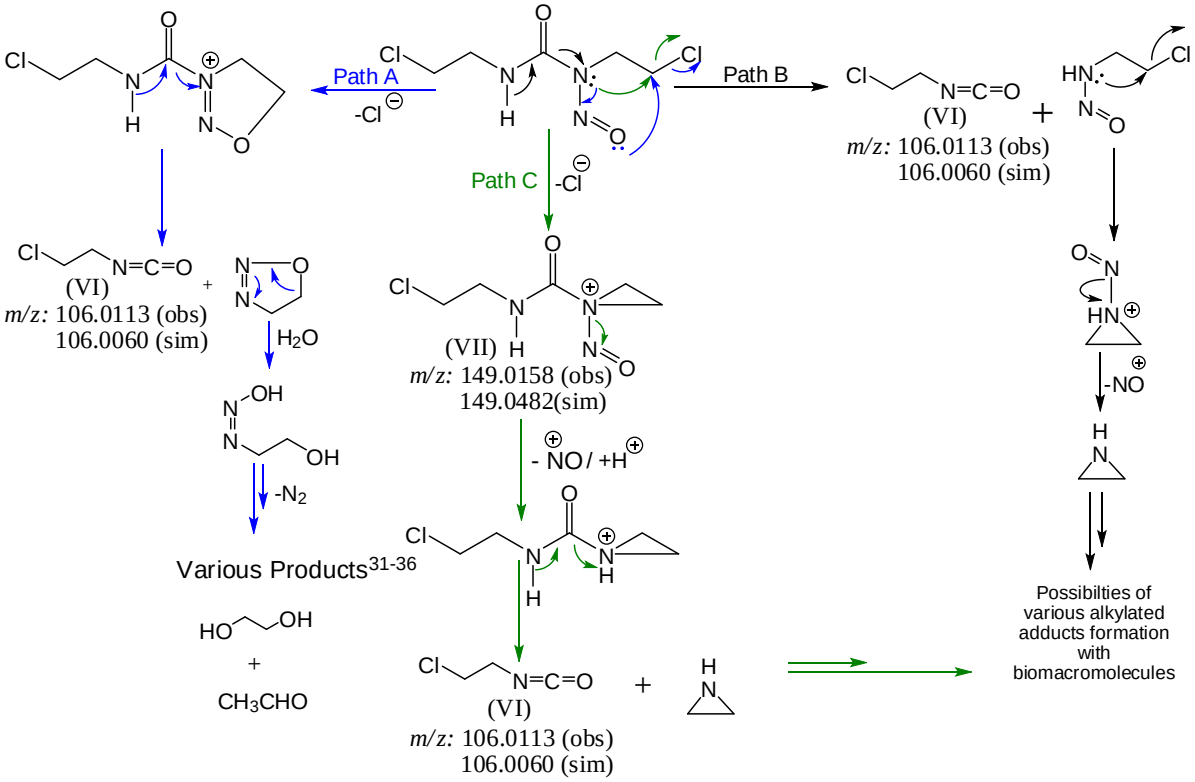

Scheme S4. Schematic representation of proposed mechanism of dissociation pathways for BCNU.

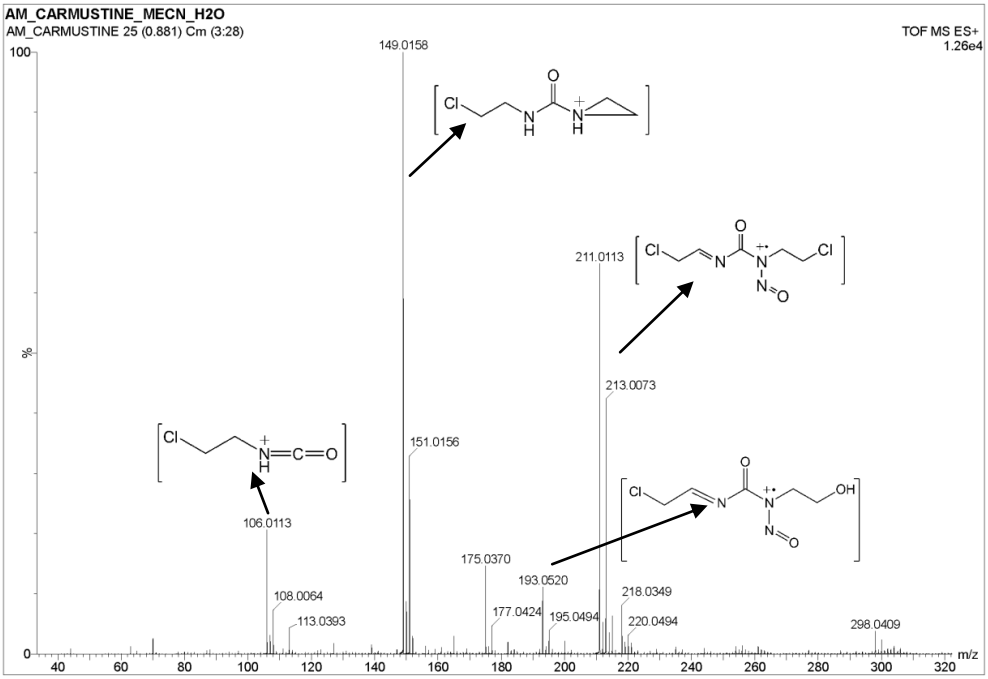

Fig. S19A ESI-MS (+ve ion mode) of BCNU in MeCN-H_2O mixture (2:1).

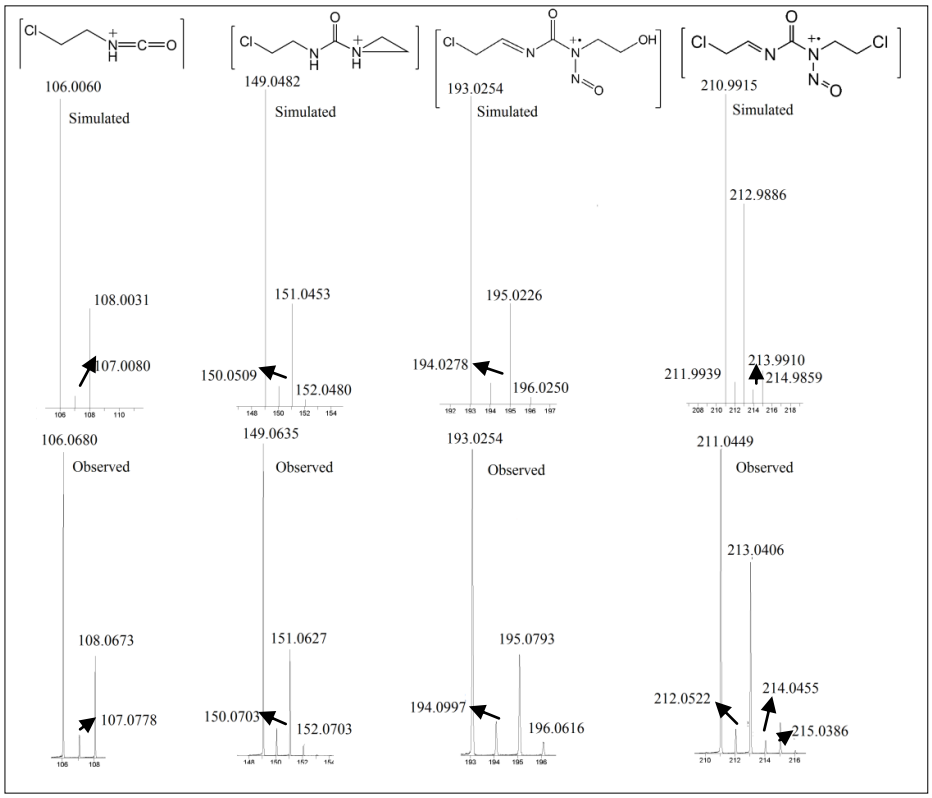

Fig. S19B Match of the isotopic distribution of the speciation of BCNU obtained in ESI-MS (+ ve mode). A comparison of experimental and calculated values are provided.

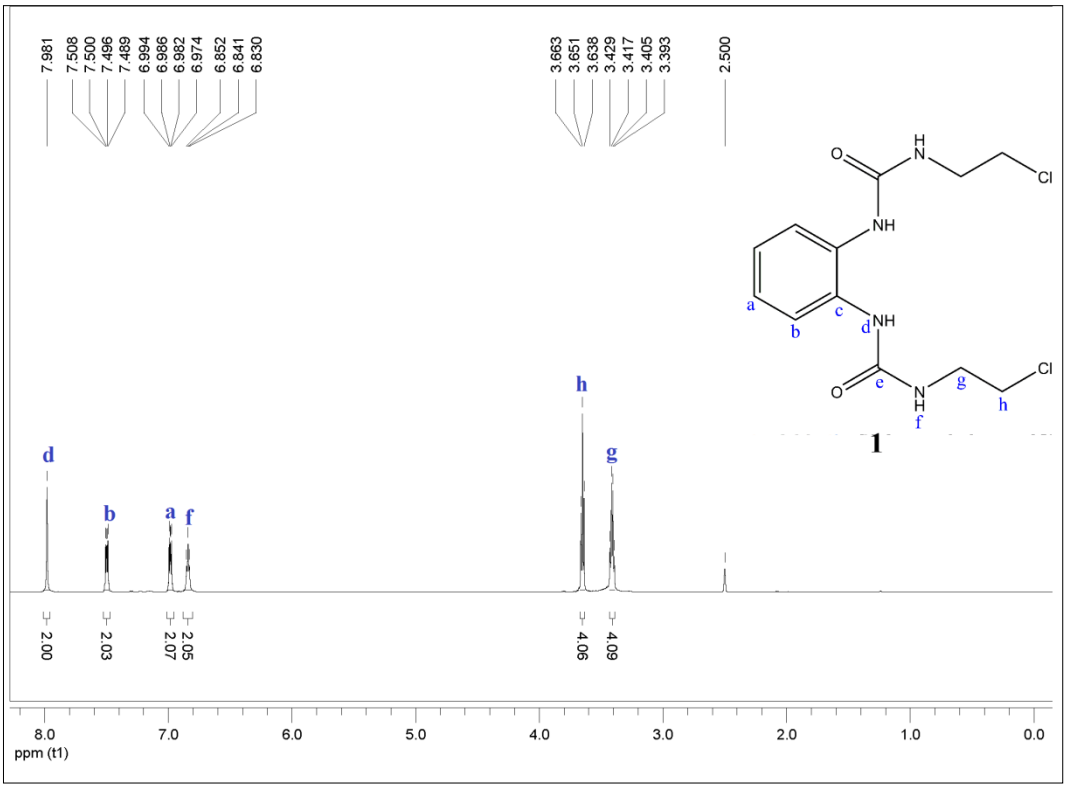

Fig. S20 ^{1}H NMR spectrum of **1** in DMSO-d_6.

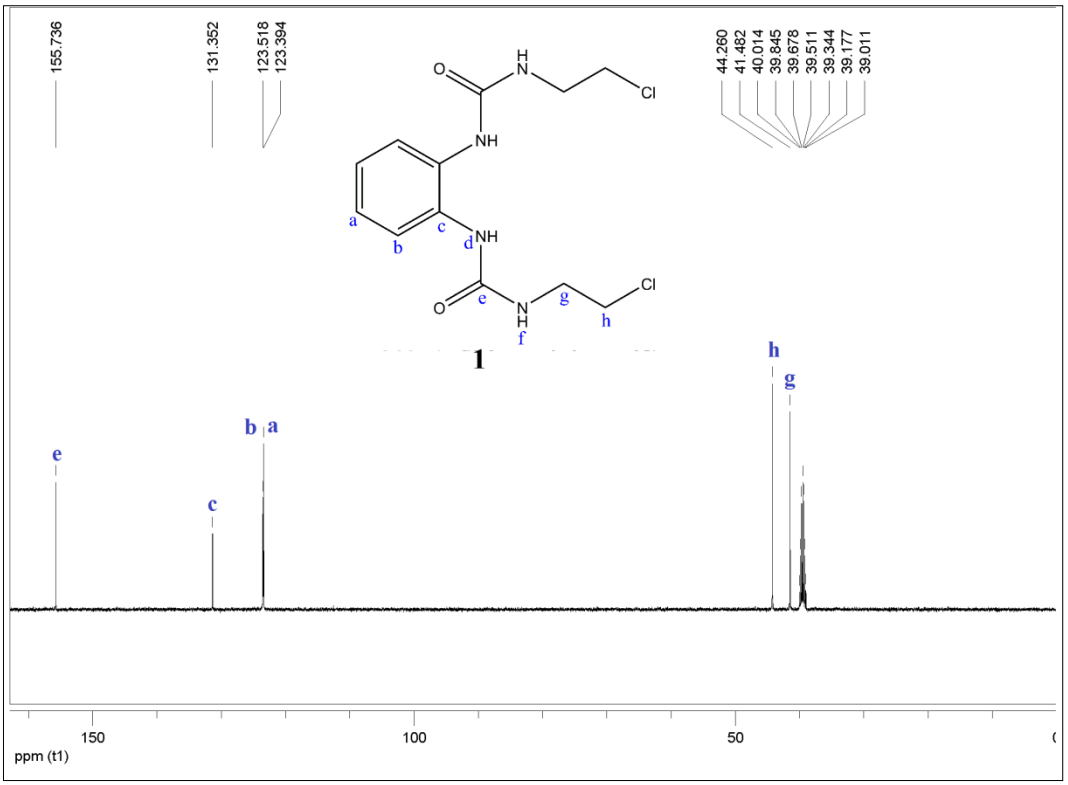

Fig. S21 ^{13}C NMR spectrum of **1** in DMSO-d_6.

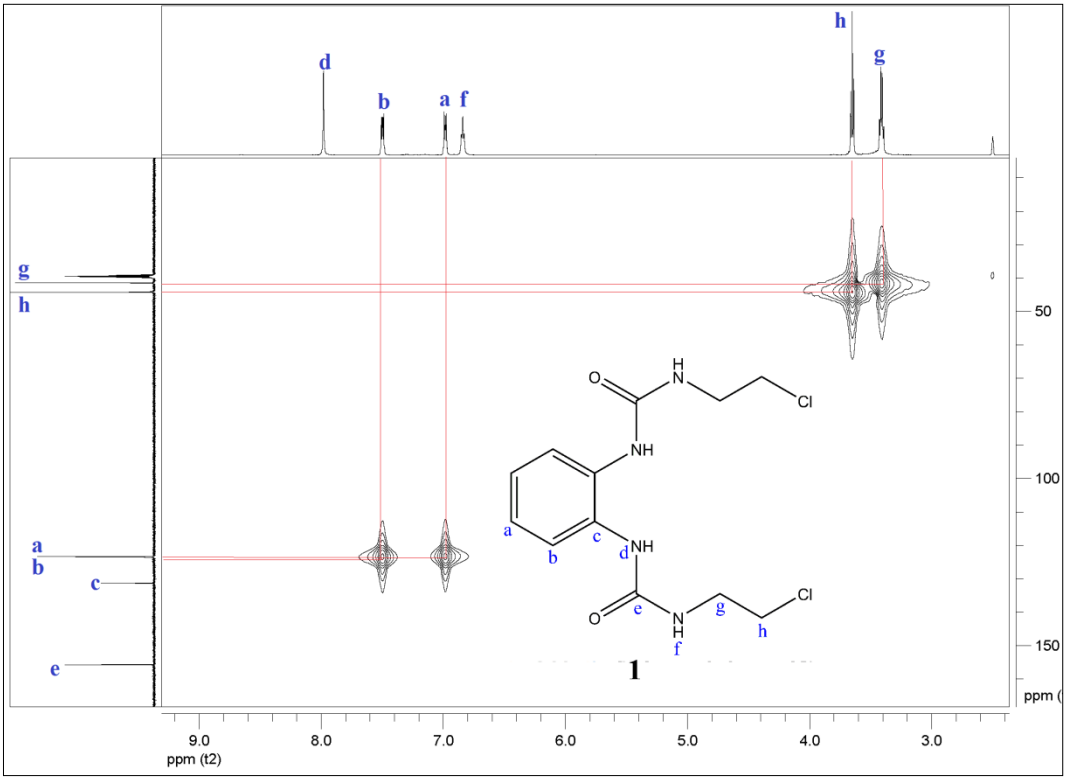

Fig. S22 HMQC spectrum of **1** in DMSO-d_6.

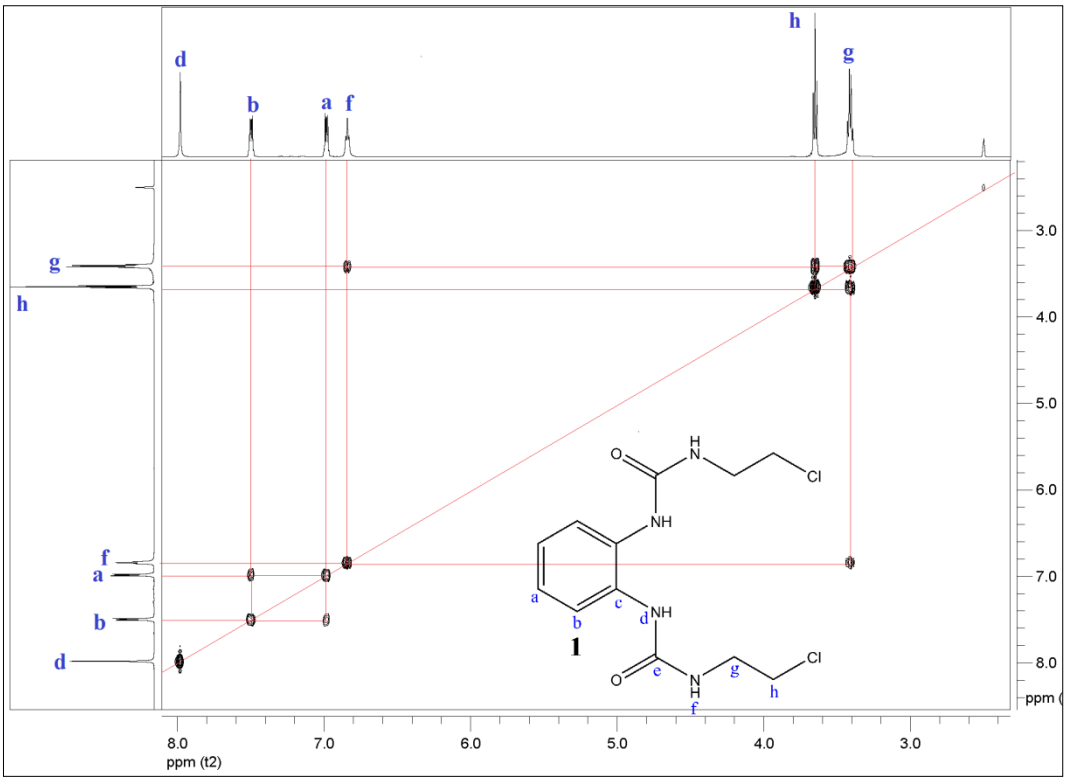

Fig. S23 COSY spectrum of **1** in DMSO-d_6.

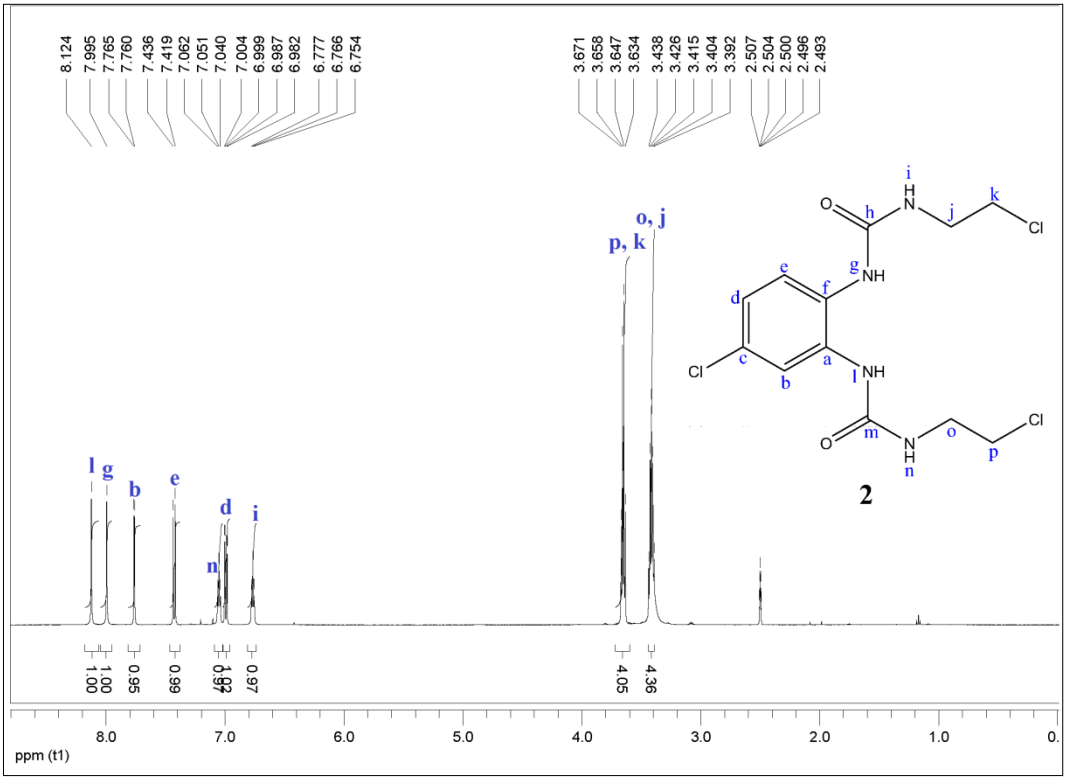

Fig. S24 ^{1}H NMR spectrum of **2** in DMSO-d_6.

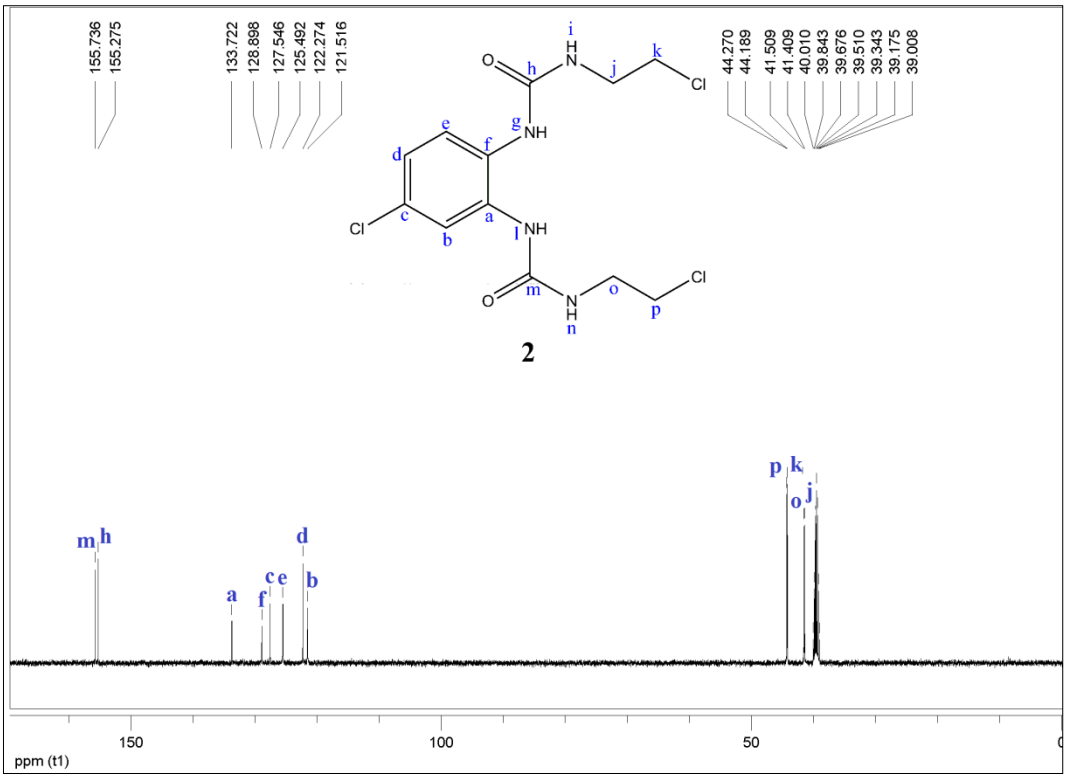

Fig. S25 ^{13}C NMR spectrum of **2** in DMSO-d_6.

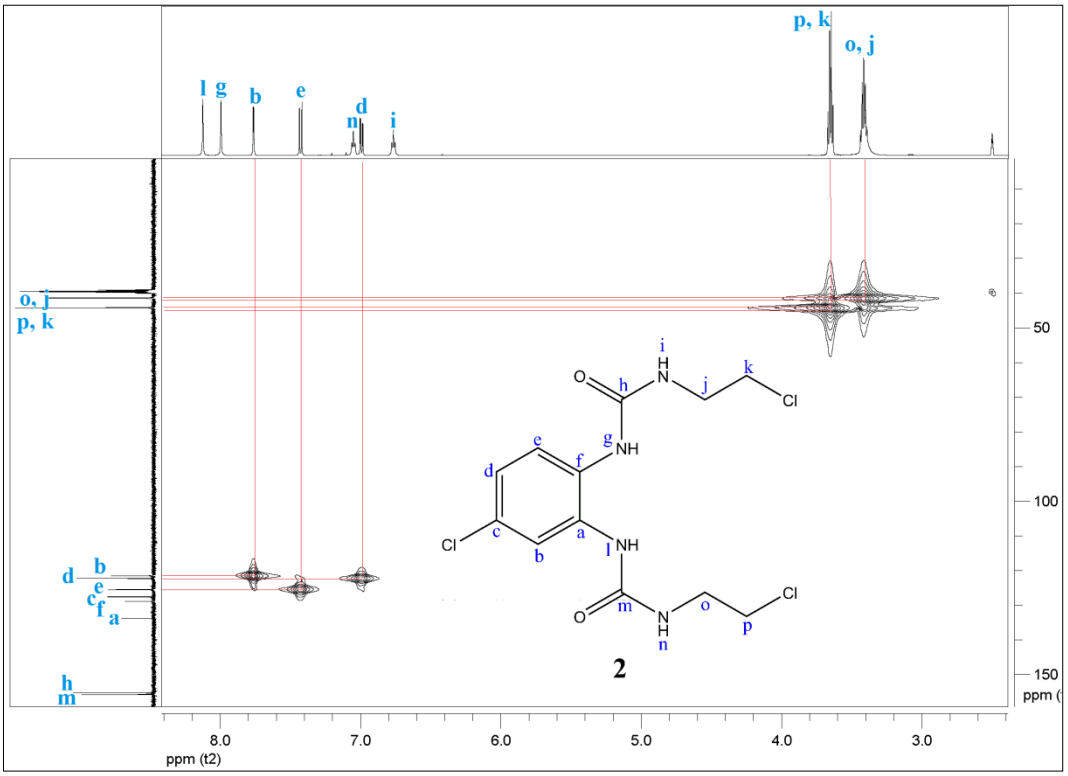

Fig. S26 HMQC spectrum of **2** in DMSO-d_6.

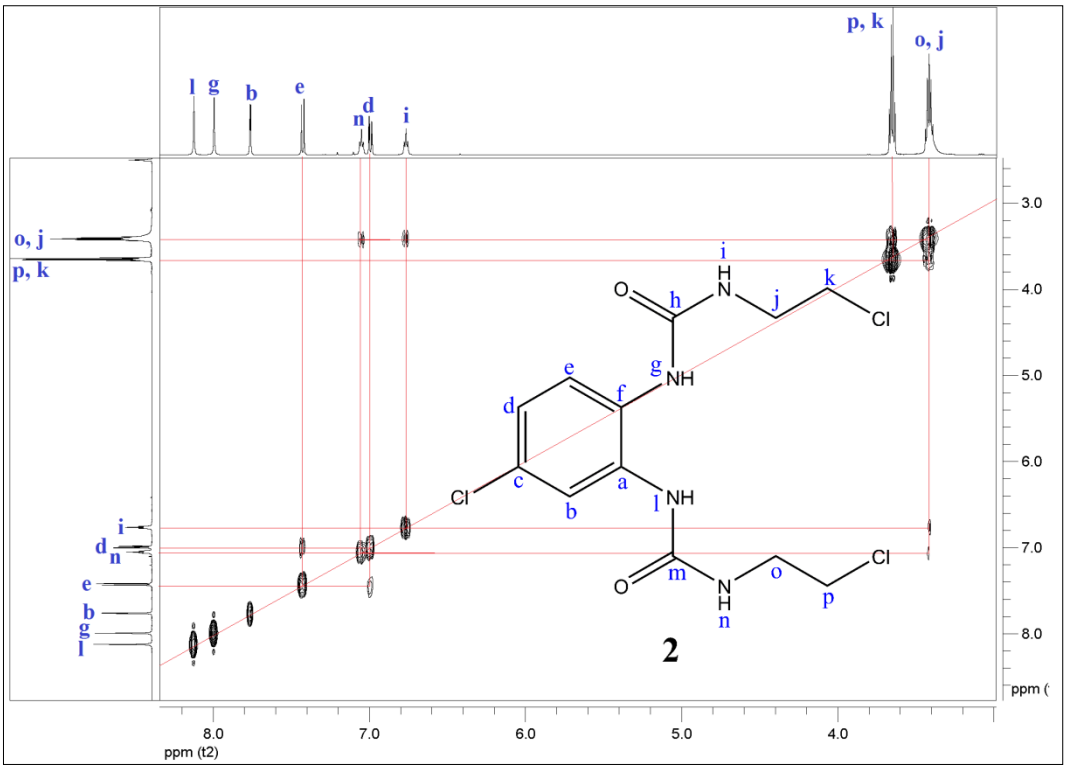

Fig. S27 COSY spectrum of **2** in DMSO-d_6.

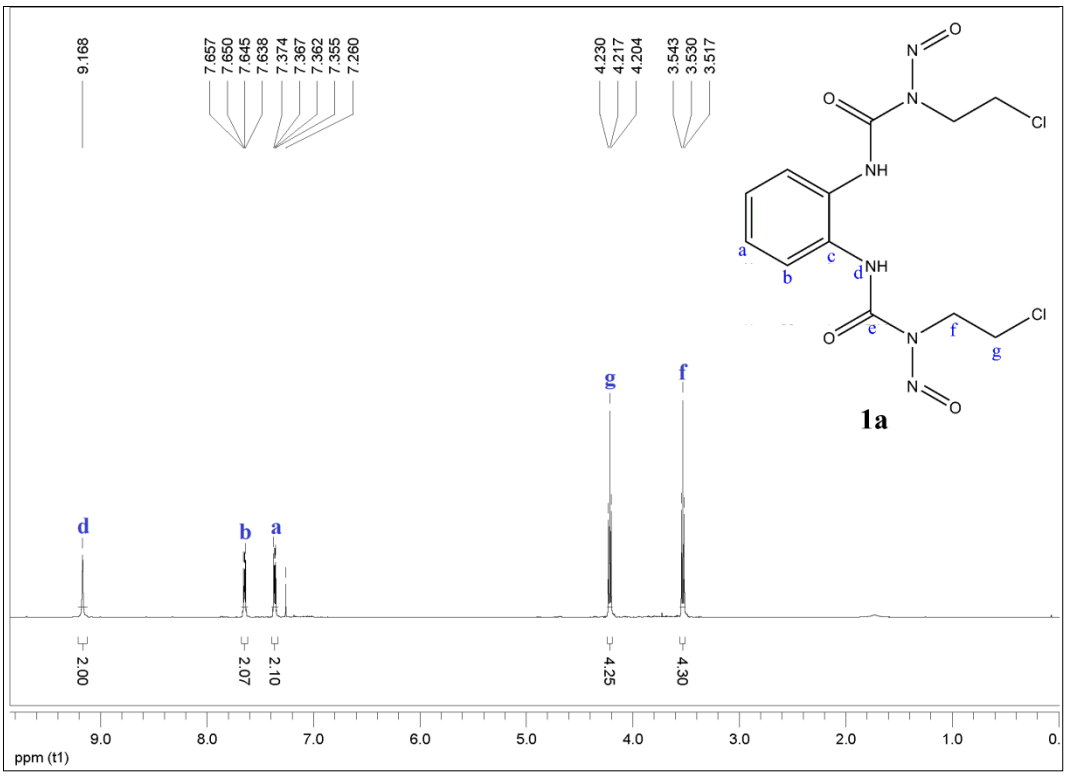

Fig. S28 ^{1}H NMR spectrum of **1a** in $CDCl_3$.

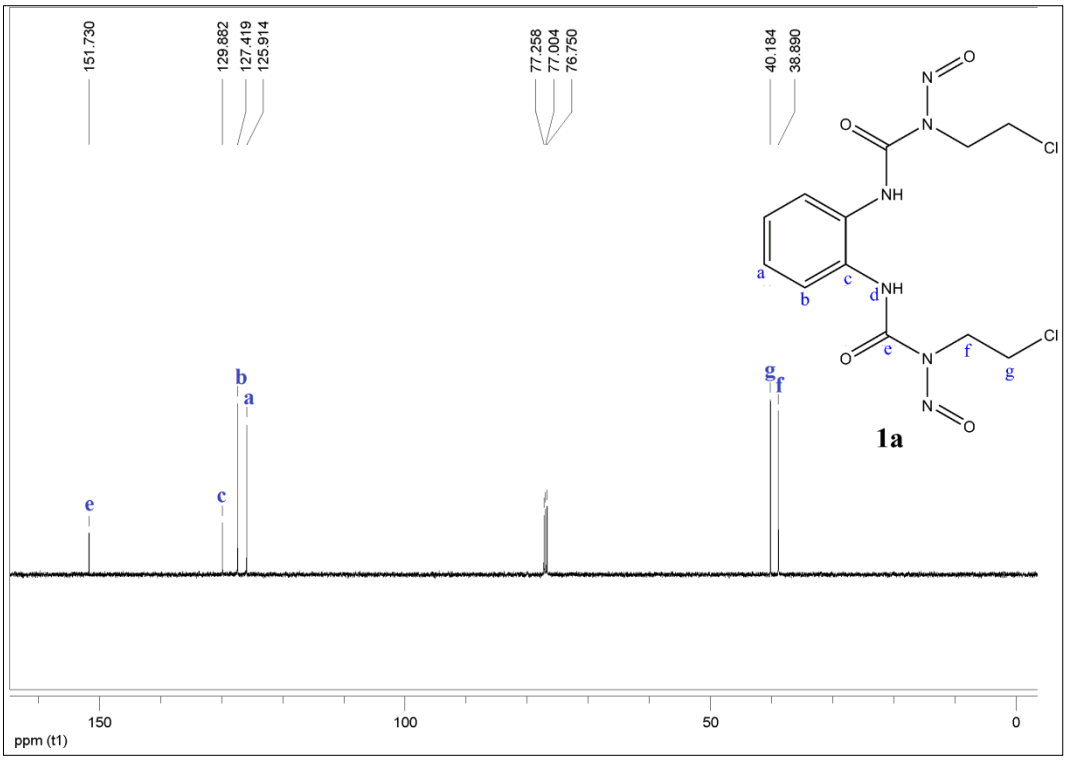

Fig. S29 ^{13}C NMR spectrum of **1a** in $CDCl_3$.

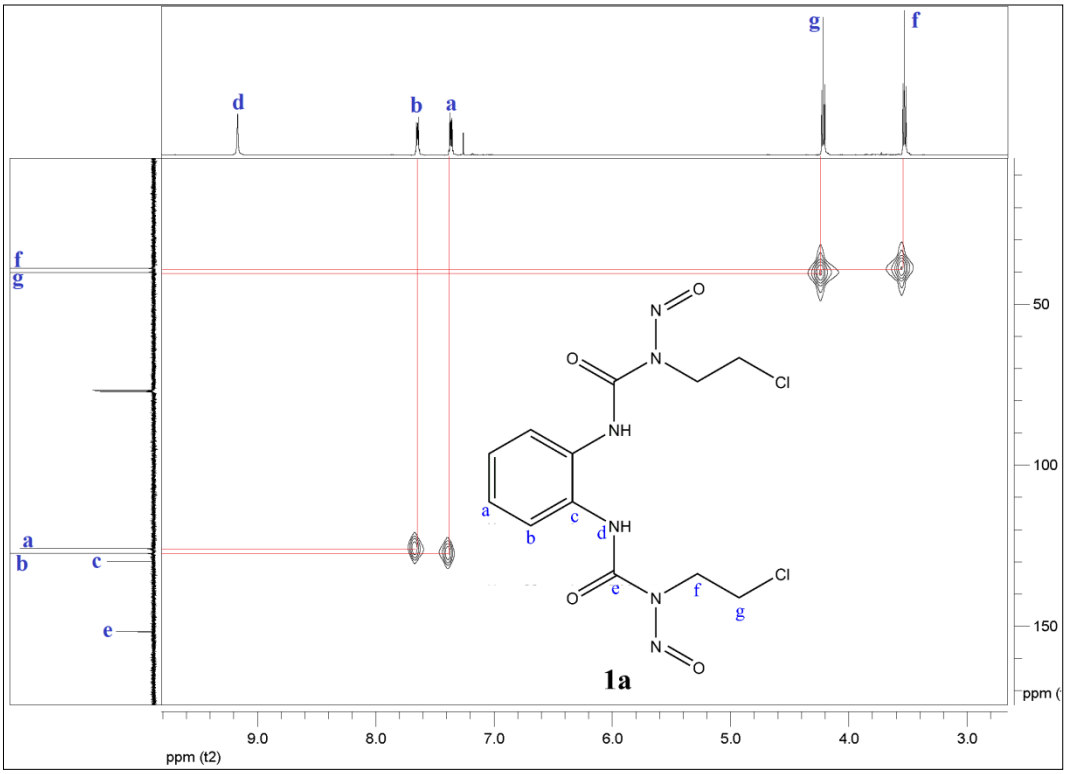

Fig. S30 HMQC spectrum of **1a** in $CDCl_3$.

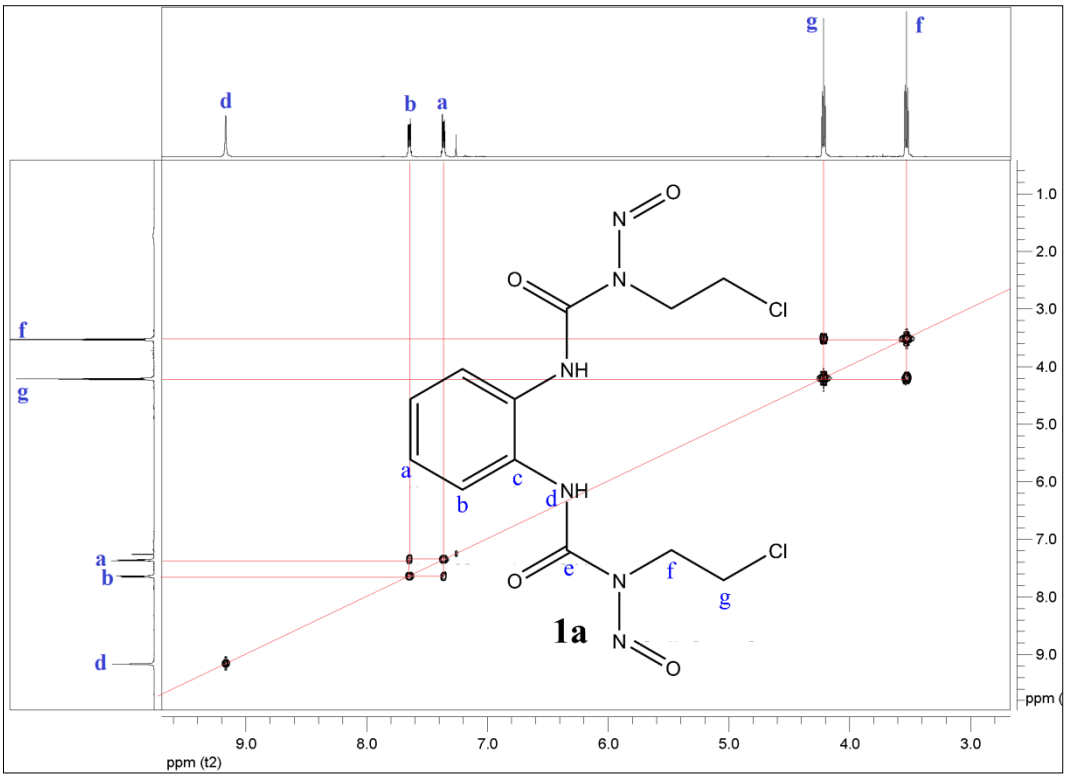

Fig. S31 COSY spectrum of **1a** in $CDCl_3$.

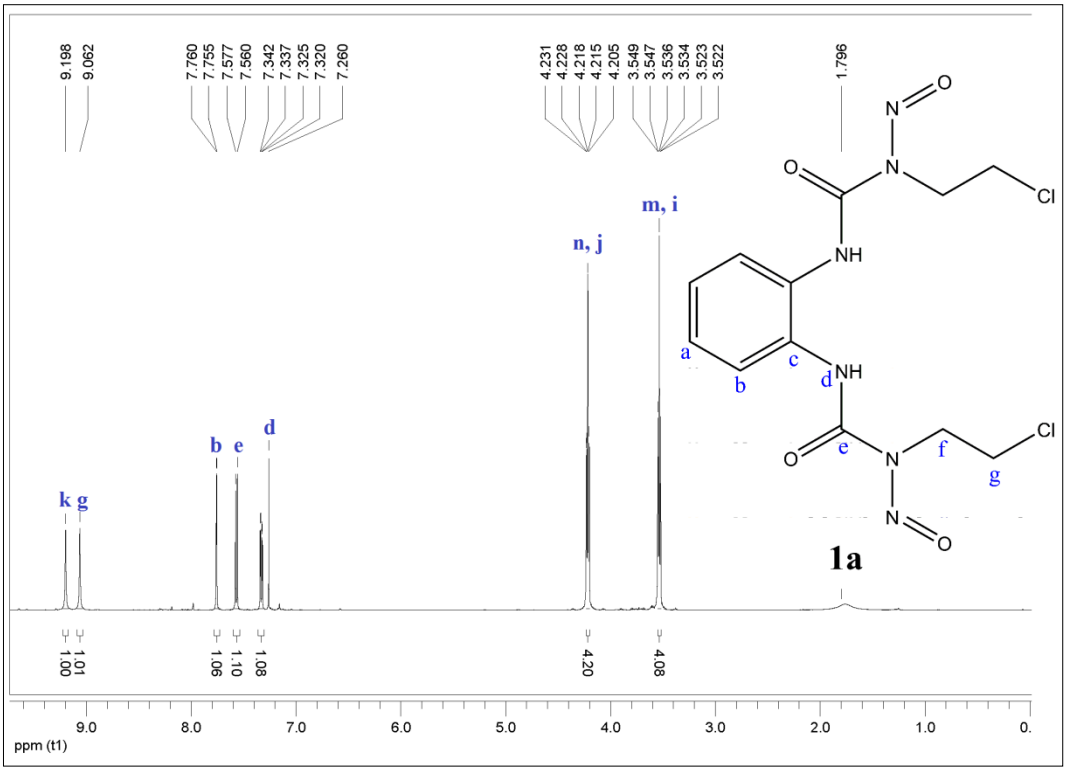

Fig. S32 ^{1}H NMR spectrum of **2a** in $CDCl_3$.

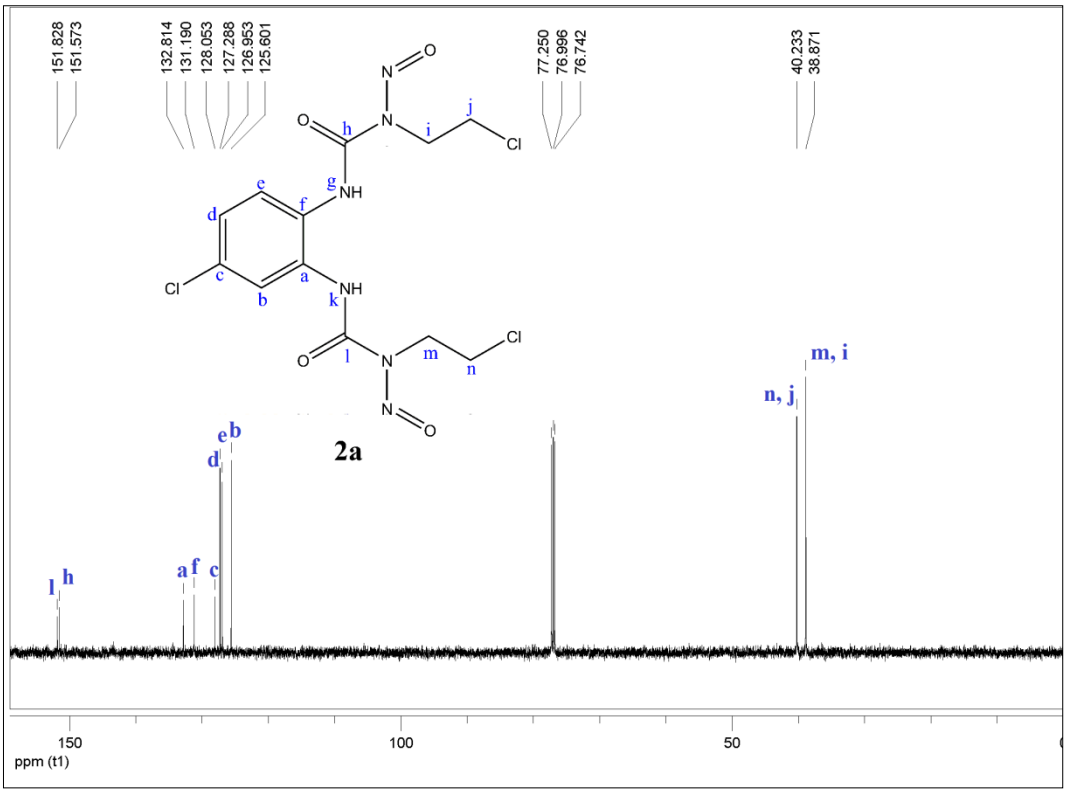

Fig. S33 ^{13}C NMR spectra of **2a** in $CDCl_3$.

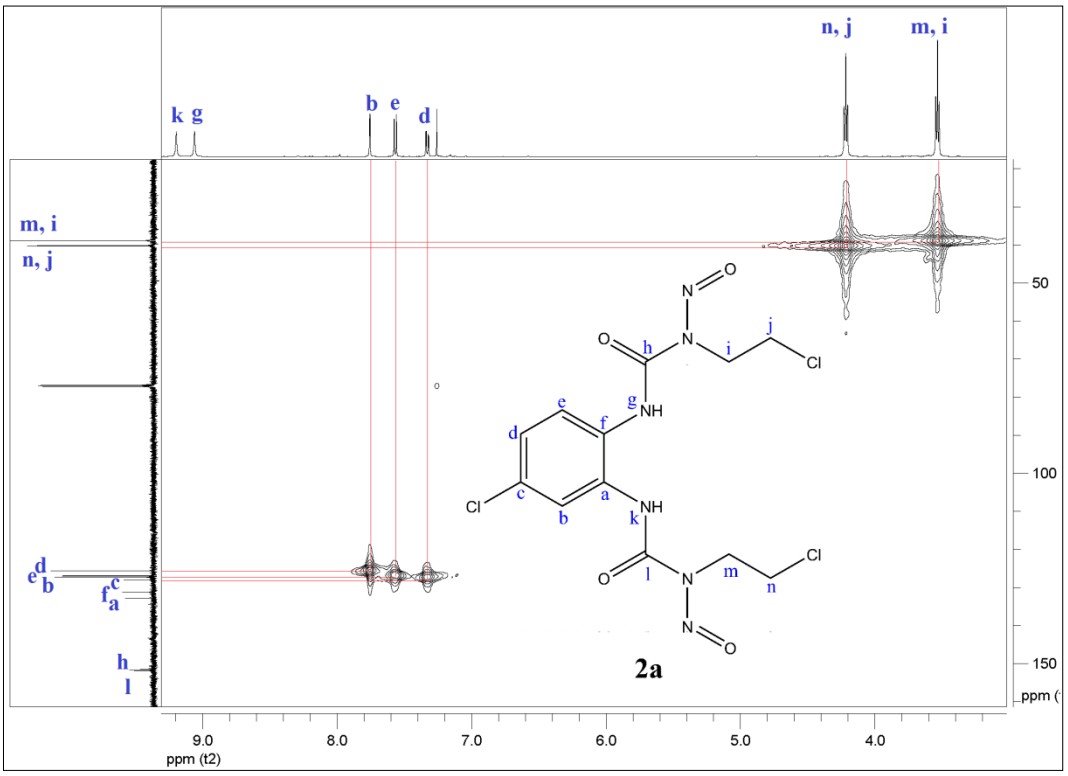

Fig. S34 HMQC spectra of **2a** in $CDCl_3$.

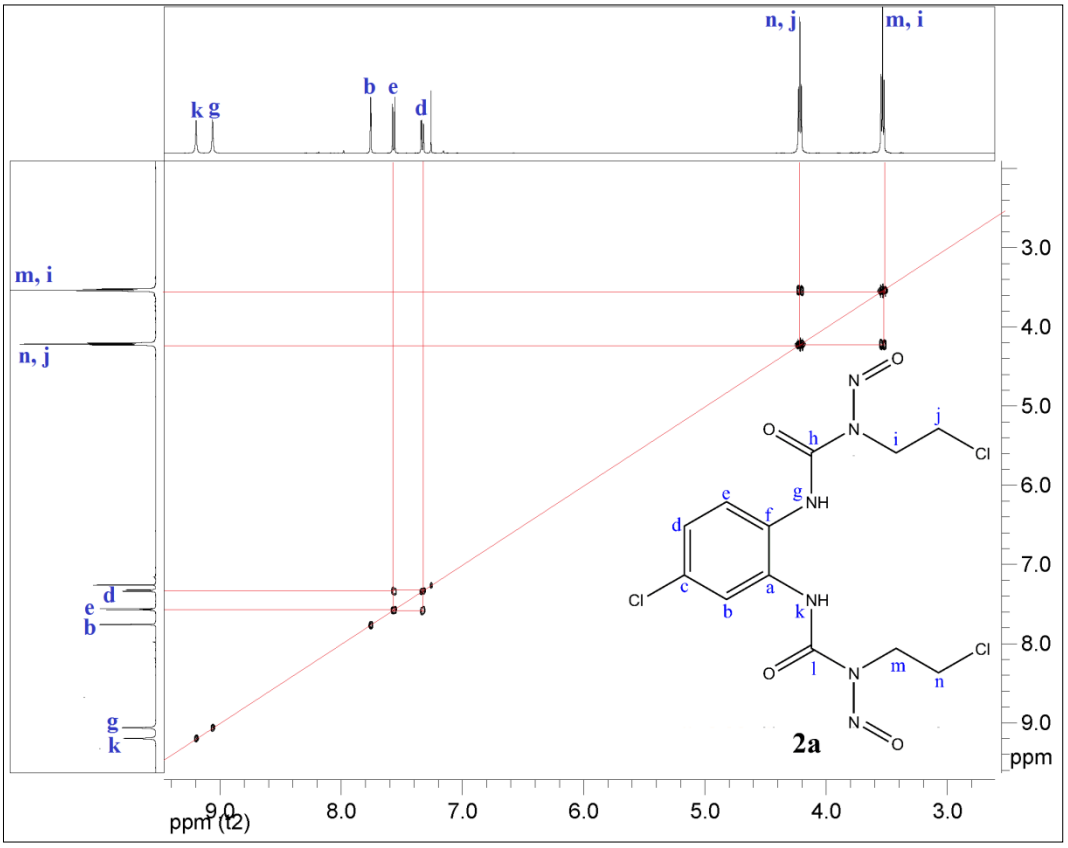

Fig. S35 COSY spectra of **2a** in $CDCl_3$.